Proceedings of the 28th IEEE
EMBS Annual International Conference
New York City, USA, Aug 30-Sept 3, 2006

Angiographic Assessment of the Performance of Flow Divertors to Treat Cerebral Aneurysms

Chander Sadasivan, Baruch B. Lieber, Liliana Cesar, Laszlo Miskolczi, Jaehoon Seong, and Ajay K. Wakhloo

Abstract— **Past clinical and experimental evidence suggests that cerebral aneurysms can be successfully excluded from the circulation solely by the endovascular placement of a flow diverting device across the aneurysm neck. These devices promote intraaneurysmal flow stasis and concomitant thrombosis by redirecting flow away from the aneurysm. To comprehensively test the efficacy of such flow divertors, we are implanting devices with three different porosities in a large cohort of elastase-induced aneurysms in rabbits. Treatment efficacy is quantified by a mathematical model that is fit to aneurysmal angiographic contrast washout curves. Results from three animals implanted with different device porosities are presented here. The model competently captures the behavior of the aneurysmal washout curves and provides reliable indices of device efficacy. Preliminary analysis indicates that immediately after implantation, the device with medium porosity performs better than the devices with lower and higher porosities.**

I. Introduction

It is estimated that intracranial aneurysms are prevalent in approximately 2% of the general population. The greatest risk that aneurysms present is that of rupture leading to subarachnoid hemorrhage (SAH). Most nontraumatic SAH cases are due to aneurysmal rupture and the annual incidence of aneurysmal SAH is about 1 per 10,000 of the population. Due to the high mortality rates (about 50%) associated with a SAH event, various treatment modalities have been proffered over the years to treat cerebral aneurysms. Surgical clipping of the aneurysm neck has been the predominant mode of treatment until recently, but is largely being replaced by endovascular coiling of the aneurysm sac because of lower associated risks and better outcome in the latter. Aneurysm coiling, however, carries its own perils especially in wide-neck or low dome-to-neck ratio aneurysms [1]. Two significant risks of coiling are intraoperative rupture of the aneurysm and coil herniation into the parent artery. Stents are increasingly being used as buttresses to maintain the coils within the aneurysm and to allow more compact coil packing in procedures involving complex aneurysms [1,2]. The increase in stent-assisted coiling procedures has largely been facilitated by technological improvements in stent design and manufacture, which have allowed the production of flexible self-expanding stents for intracranial use.

Depending on aneurysm size, location, and associated local hemodynamics, it is also possible to achieve aneurysm occlusion by placing a stent across the aneurysm neck without any assisting devices [3]. The stent impedes transfer of flow momentum into the aneurysm by diverting flow into the parent artery. This creates intraaneurysmal flow stasis, which promotes thrombosis and aneurysm occlusion. Although this concept has gained sufficient validation through both clinical and experimental data accumulated over the past decade, conclusive evidence as to its effectiveness is still lacking.

We are currently evaluating the efficacy of flow divertors in treating cerebral aneurysms by implanting these devices in a large cohort of experimental animals. The elastase-induced aneurysm model in rabbits has been chosen for this purpose. Device porosity is known to be a significant parameter determining treatment outcome and we are implanting devices with three different porosity values based on past experience [4]. We have previously developed a method to quantify the effectiveness of flow divertors in treating cerebral aneurysms by analyzing angiographic data [5]. The temporal variation in angiographic contrast intensity within the aneurysm is obtained and a mathematical model is fit to the resulting washout curve. Three of the model parameters act as indices of treatment efficacy, and possibly, as predictors of long-term outcome. This angiographic analysis will be carried out and the results assessed along with histological data from explants obtained during follow-up time points (three weeks to six months). The angiographic data and results from three animals implanted with devices having three different porosities are presented here.

II. Methods

A. Animal Experiments

The elastase-induced saccular aneurysm model in rabbits

Manuscript received April 3, 2006. This work was supported by the National Institutes of Health under grant number R01 NS045753-01A1 to BBL.

C. Sadasivan is with the Department of Biomedical Engineering, University of Miami, Coral Gables, FL 33146 USA (Tel: 305-284-2059; Fax: 305-284-6494; E-mail: c.sadasivan@umiami.edu).

B.B. Lieber and J. Seong are with the Department of Biomedical Engineering, University of Miami, Coral Gables, FL 33146 USA (E-mails: blieber@miami.edu; j.seong@miami.edu).

L. Cesar is with the Endovascular Research Center, Vascular Biology Institute, University of Miami, Miami, FL 33136 USA (E-mail: LCesar@med.miami.edu).

L. Miskolczi was with the Department of Radiology, University of Miami, Miami, FL 33136. He is currently with the Memorial Healthcare System, Hollywood, FL 33021 USA (E-mail: laszlo@mad.scientist.com).

A.K. Wakhloo is with the Department of Radiology, University of Massachusetts Medical School, Worcester, MA 02481 USA (E-mail: WakhlooA@ummhc.org).

[6] is currently the best *in vivo* model for testing relevant endovascular treatment modalities. Over the past three years, we have gained sufficient experience with this model to achieve low attrition rates (approximately 5%). The technique we use to create these aneurysms is described elsewhere [7]. Essentially, the right common carotid artery is ligated distally and occluded by a balloon proximally. Incubation of elastase within the isolated section degrades the arterial wall leaving a pouch-like formation at the base of the artery that simulates a cerebral aneurysm. After allowing the aneurysm to mature for three weeks, self-expanding flow divertors are introduced via a right transfemoral approach and deployed across the aneurysm neck under fluoroscopic guidance. The devices are positioned such that, ideally, the post-deployment landing zones on either side of the aneurysm are equal.

Before a device is deployed, a 4F catheter is placed in the aortic arch and 5cc of pure angiographic contrast (Visipaque™, 320 mgI/ml, GE Healthcare, UK) are injected through it at a rate of 2 cc/s. Angiographic images are acquired during contrast injection at a rate of 30 frames per second for 20 seconds (cardiac mode, Polytron TOP, Siemens, Forchheim, Germany). Immediately after device deployment, another high-speed angiographic acquisition with power injection of contrast is carried out using identical imaging and injection parameters. The contrast injector is programmed such that injection occurs 1.5 to 2 seconds after start of image acquisition. A dime is placed on the rabbit within the field of view for calibration purposes.

B. Image Analysis

The angiographic sequences acquired before and after device deployment are then converted using Matlab® (The Mathworks, Natick, MA) from DICOM to a bitmap format for processing on a Windows PC. All the image processing and subsequent analysis was done in Matlab®. Each angiographic sequence consists of 601 native (unsubtracted) frames that have a pixel resolution of 512×512. During image acquisition, the animal lies supine with the cranial direction at the top of the image. Due to its proximity to the thorax, there is substantial movement of the aneurysm-parent vessel complex in the cranial-caudal direction, which is largely synchronous with the respiratory cycle of the animal. Logarithmic subtraction of the angiographic sequences was thus performed based on the respiratory cycle. A set of frames comprising one respiratory cycle was selected from the time period before contrast injection. This set of images formed the mask based on which the corresponding images in each subsequent respiratory cycle were subtracted.

When a device is deployed, it increases the radius of curvature of the parent artery (Fig. 1). The radius of curvature of the artery was calculated before and after deployment as an estimate of the longitudinal stiffness of the device. An image where the parent artery was opacified was selected from both the pre- and post-deployment sequences

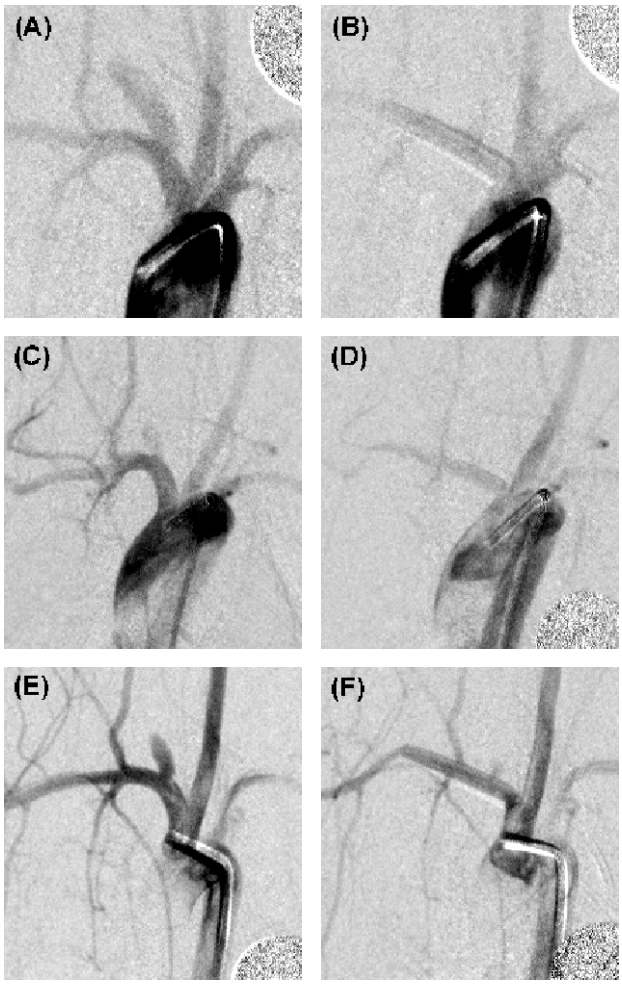

Fig. 1. Angiograms showing maximum opacification of the aneurysm. Left column: pre-device implantation; right column: immediately post-device implantation; (A) and (B) high porosity device; (C) and (D) medium porosity device; (E) and (F) low porosity device

and a section of parent artery at the aneurysm was manually isolated. A binary image of this arterial section is formed by thresholding and the centerline calculated by morphological thinning. The equation of a circle is fit to this centerline in the least-squares sense to give the representative radius of curvature of the artery.

Fig. 1 shows the images with peak opacification of the aneurysm before and after device deployment in three cases representing different device porosities. A region of interest (ROI) tracing the aneurysm circumference was manually delineated in each of these images. A set of images comprising one respiratory cycle where the parent artery is opacified was then selected and each of these images was locally thresholded to get the vertical location of the top edge of the artery. Based on this position vector, the ROI was moved in the cranial-caudal direction in accordance with the aneurysm position. The average grayscale value within the aneurysm (sum of grayscale value of pixels in ROI/number of pixels in ROI) was calculated for each image and then inverted to give the aneurysmal washout curves.

C. Mathematical Modeling

The point of significant rise in the washout curve was shifted to the origin and the curve normalized to give the temporal variation in the normalized average inverted grayscale value (NAIGV). This curve was then mathematically modeled based on (1).

$$f(t) = \rho_{conv} \int_0^t \frac{1}{\sigma\sqrt{2\pi}} e^{-\frac{(\eta-\mu)^2}{2\sigma^2}} \times \frac{1}{\tau_{conv}} e^{-\frac{t-\eta}{\tau_{conv}}} d\eta + \rho_{disp} \left[\int_0^t \frac{1}{\sigma\sqrt{2\pi}} e^{-\frac{(\eta-\mu)^2}{2\sigma^2}} d\eta - (1 - e^{-\frac{t}{\tau_{disp}}}) \right] \quad (1)$$

This mathematical model utilizes parameters that can be associated with the hemodynamics of the aneurysm-parent vessel complex as it represents the washout curve as a sum of convective and dispersive components (first and second parts of the equation, respectively) [5]. The convective part is a lagged normal distribution and the dispersive part is the sum of a sigmoid curve and an exponential decay. ρ_{conv} and ρ_{disp} represent the relative magnitudes of convective and dispersive transport, respectively, while τ_{conv} and τ_{disp} are the corresponding time constants. The parameters σ and μ characterize the method of contrast injection. After device implantation, intraaneurysmal flow becomes relatively sluggish, indicating that dispersive transport tends to dominate over the convective mode of transport. An increase in the amplitude of the dispersive component (ρ_{disp}) and in both of the time constants (τ_{conv} and τ_{disp}) should thus be expected post-device deployment. Correspondingly, the value of ρ_{conv} is expected to reduce. The magnitude of these changes may be used as an estimate to compare the efficacy of one flow divertor over another.

III. Results

There were no visually identifiable errors in the movement of the vasculature of interest after the subtraction process. To quantify the error in subtraction, all the mask and contrast images were segmented to exclude the contrast-enhanced regions based on the maximum intensity projection of the entire sequence of images. As artifacts after subtraction occur mostly due to the presence of object edges [8], an edge detection operation based on the Laplacian of Gaussian method was performed on the images prior to segmentation. The percentage of non-zero pixels in the difference image (contrast – mask image) to total number of pixels was used as an estimate of the error in subtraction. For the six cases presented here, the average of this value ranged from 1.6% to 5.7% with corresponding standard deviations of 0.1% and 0.7%. In some cases, the parent artery was not completely opacified due to which the calculated position vector did not displace the ROI in tune with the aneurysm movement. In such cases, a position vector was selected by manually choosing the vertical location of the aneurysm over one respiratory cycle. Fig. 2 shows the model-fits to the aneurysmal washout curves obtained before and after device implantation for the low porosity device. Table 1 gives the parameter values obtained after fitting the mathematical model to the washout data for all three cases. The amplitudes of convective and dispersive transport are given as percentages of total model amplitude. The last column of Table 1 includes the percentage increase in the radius of curvature of the parent artery after device deployment.

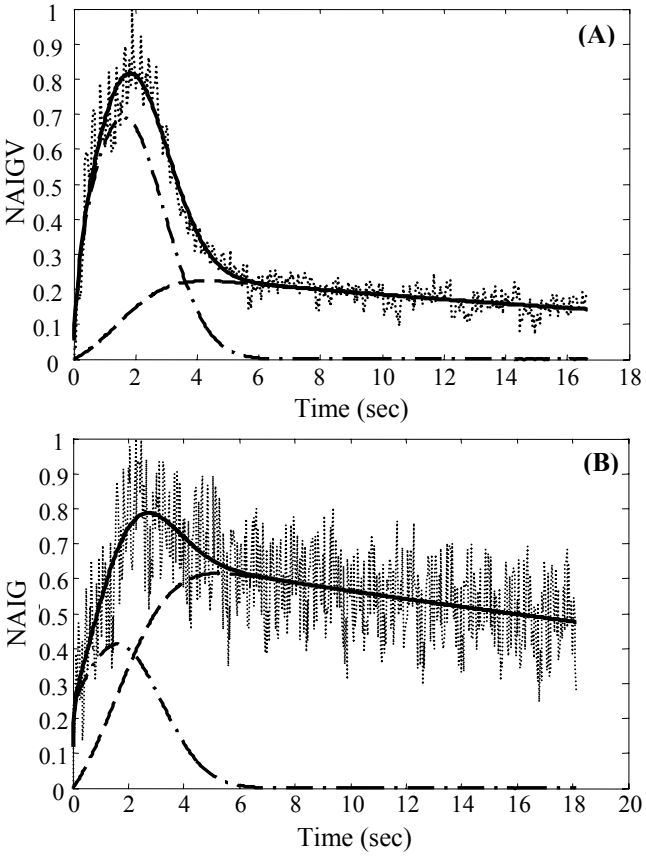

Fig. 2. Model-fits (solid lines) of (A) pre-, and (B) post-device implantation washout curves (dotted lines) for the low porosity device. The convective (dash-dot lines) and dispersive (dash lines) components of the model are indicated. NAIGV: Normalized Average Inverted Grayscale Value. Plots (A) and (B) correspond to Fig. 1(E) and Fig. 1(F), respectively.

TABLE 1. OPTIMIZED VALUES OF RELEVANT PARAMETERS

Device Porosity	DSA Acquisition	ρ_{conv} (%)	ρ_{disp} (%)	τ_{disp}	R (%)
High	Pre-Implant	60	40	72.0	806
	Post-Implant	33.8	66.2	21.2	
Medium	Pre-Implant	52.2	47.8	19.8	925
	Post-Implant	37.2	62.8	270.8	
Low	Pre-Implant	75.5	24.5	33.0	1076
	Post-Implant	40.2	59.8	59.5	

ρ_{conv} and ρ_{disp}: proportion of convective and dispersive transport, respectively; τ_{disp}: time constant of dispersive transport; R: percentage increase in radius of curvature of artery after device deployment; Pre-: immediately before device implantation; Post-: immediately after device implantation.

IV. Discussion

As in the example of Fig. 2, the model faithfully captured the trend of all the washout curves. The parameters representing the dispersive component of flow increased immediately post-device deployment, while the amplitude of convective transport decreased. The device with high porosity does not restrict flow into the aneurysm as much as the other two devices and the dispersive time constant is lower post-deployment than before deployment. It is noted, however, that the proportion of dispersive transport increases by about 65% in this case while the convective transport decreases by about 44%, implying that intraaneurysmal flow stasis is induced. Overall assessment of Table 1 along with the angiograms shown in Fig. 1 suggests that the device with medium porosity performs better than either of the other two devices. Increasing the device porosity can reduce its longitudinal stiffness and provide increased maneuverability as evidenced by the last column of Table 1.

Both the subtraction process and accuracy in determining the position vector for displacing the ROI affect the smoothness of the washout curves. The subtraction process used here assumes that the respiratory rate remains constant to the order of a single frame (1/30 seconds) over 20 seconds of acquisition time. Although the rabbits were stabilized as much as possible, changes in their respiratory rates during the procedure are inevitable. The motion of the aneurysm is also affected by cardiac pulsatility, and this relation is difficult to take into account during subtraction. As noted in the results section, however, the errors introduced by the subtraction process are low. The device introduces a ghost artifact during subtraction of angiographic sequences acquired post-deployment. Also, the aneurysm is significantly occluded (angiographically) immediately after a device is deployed leaving only a neck remnant in some cases. When delineating a ROI around this remnant, care had to be taken to ensure that the ROI did not incorporate the ghost artifact. The position vector of the ROI is dependent on the degree of opacification of the parent artery and some inaccuracies in moving the ROI are to be expected. Although these circumstances reduce the fidelity of the resultant washout curve, the subtraction process and ROI tracking were visually evaluated, and reiterated if necessary, to ensure that these errors are minimized.

Implantation of bare stents across elastase-induced aneurysms in ten rabbits has previously been performed with a maximum follow-up time point of three months [2]. Neointimal proliferation was observed at three month follow-up, which may be due to the fact that balloon-expandable stents were used. Histological evaluation at this time point showed intraaneurysmal thrombotic material in 4 out of 5 animals [2]. Treatment efficacy was evaluated angiographically only by visualization and no quantitative method was used. Our mathematical model provides robust quantitative indices of stent efficacy that may act as predictors of long term treatment outcome. Preliminary data at three-week follow up show complete angiographic occlusion of the aneurysm with the medium and low porosity devices and a patent parent artery with intraaneurysmal thrombotic material on histology. Also, three month follow-up for a medium porosity device shows angiographically patent parent artery and obliterated aneurysm (Fig. 3). Results thus far indicate that the medium porosity device may perform better than the devices with lower or higher porosity. However, long term data need to be analyzed before any conclusive statements can be drawn.

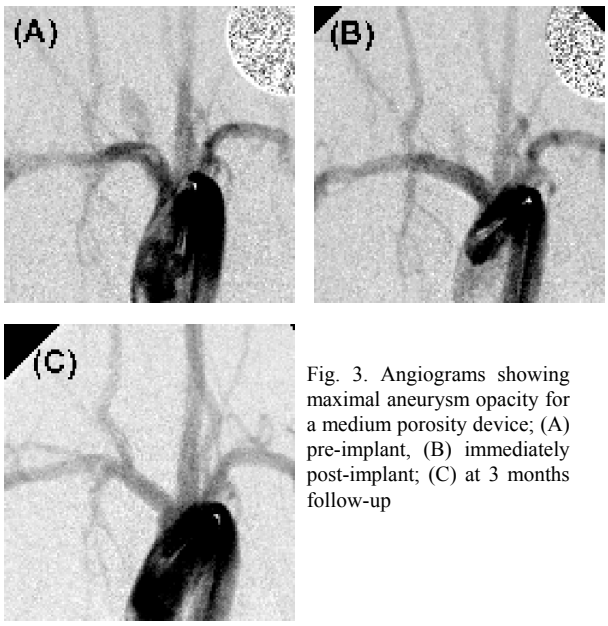

Fig. 3. Angiograms showing maximal aneurysm opacity for a medium porosity device; (A) pre-implant, (B) immediately post-implant; (C) at 3 months follow-up

References

[1] P. Lylyk, A. Ferrario, B. Pasbon, C. Miranda, and G. Doroszuk, "Buenos Aires experience with the Neuroform self-expanding stent for the treatment of intracranial aneurysms," *J. Neurosurg.*, 102(2), pp. 235-241, Feb. 2005.

[2] T. Krings, F.J. Hans, W. Moller-Hartmann, A. Brunn, R. Thiex, T. Schmitz-Rode, P. Verken, K. Scherer, H. Dreeskamp, K.P. Stein, J. Gilsbach, and A. Thron, "Treatment of experimentally induced aneurysms with stents," *Neurosurgery*, 56(6), pp. 1347-1359, Jun. 2005.

[3] A.K. Wakhloo, F. Schellhammer, J. de Vries, J. Haberstroh, and M. Schumacher, "Self-expanding and balloon-expandable stents in the treatment of carotid aneurysms: an experimental study in a canine model," *AJNR Am. J. Neuroradiol.*, 15(3), pp. 493-502, Mar. 1994.

[4] B.B. Lieber, A.P. Stancampiano, and A.K. Wakhloo, "Alteration of hemodynamics in aneurysm models by stenting: influence of stent porosity," *Ann. Biomed. Eng.*, 25(3), pp. 460-469, May-Jun. 1997.

[5] C. Sadasivan, B.B. Lieber, M.J. Gounis, D.K. Lopes, and L.N. Hopkins, "Angiographic quantification of contrast medium washout from cerebral aneurysms after stent placement," *AJNR Am. J. Neuroradiol.*, 23(7), pp. 1214-1221, Aug. 2002.

[6] T.A. Altes, H.J. Cloft, J.G. Short, A. DeGast, H.M. Do, G.A. Helm, D.F. Kallmes, "Creation of saccular aneurysms in the rabbit: a model suitable for testing endovascular devices," *AJR Am. J. Roentgenol.*, 174(2), pp. 349-354, Feb. 2000.

[7] L. Miskolczi, M.J. Gounis, M. Onizuka, L. Cesar, B.B. Lieber, A.K. Wakhloo, and C.A. Anaya, "Elastase-induced saccular aneurysms in rabbits: Instructions "for the rest of us", in *Proc. 42nd Annual Meeting, American Society of Neuroradiology*, Seattle, 2004, pp. 352.

[8] E.H. Meijering, W.J. Niesssen, and M.A. Viergever, "Retrospective motion correction in digital subtraction angiography: a review," *IEEE Trans. Med. Imaging.*, 18(1), pp. 2-21, Jan. 1999.